On the presence of high nitrite (NO_2^-) in coarse particles at Mt. Qomolangma

Zhongyi Zhang[1, 2], Chunxiang Ye[3], Yichao Wu[1], Tao Zhou[4], Pengfei Chen[5,6], Shichang Kang[5,6], Chong Zhang[3], Zhuang Jiang[1], Lei Geng[1, 2, 4*]

[1]Deep Space Exploration Laboratory/School of Earth and Space Sciences, University of Science and Technology of China, Hefei 230026, Anhui, China

[2]CAS Center for Excellence in Comparative Planetology, University of Science and Technology of China, Hefei 230026, Anhui, China

[3]SKL-ESPC & SEPKL-AERM, College of Environmental Sciences and Engineering, and Center for Environment and Science, Peking University, Beijing 100871, China

[4]National Key Laboratory of Deep Space Exploration, Hefei, 230088, Anhui, China.

[5]Key Laboratory of Cryospheric Science and Frozen Soil Engineering, Northwest Institute of Eco-Environment and Resources, Chinese Academy of Sciences; Lanzhou, 730000, Gansu, China

[6]University of Chinese Academy of Sciences; Beijing, 100049, China

* *Correspondence to*: Lei Geng (Email: genglei@ustc.edu.cn; Tel: +86-0551-63600015)

Abstract

Atmospheric reactive nitrogen cycling, with nitrous acid (HONO) and particulate nitrite (NO_2^-) as important intermediates, is crucial for maintaining the atmospheric oxidation capacity of background atmosphere on the Tibetan Plateau. During an eleven-day field campaign at the Base Camp of Mt. Qomolangma in spring of 2022, we observed significant enrichments of NO_2^- in total suspended particulate (TSP) with a mean concentration of 375 ± 386 ng m^{-3}, while NO_2^- was absent in fine particles ($PM_{2.5}$). The comparison revealed that NO_2^- predominately exists in coarse particles. Local surface soil at the sampling site also exhibited high levels of NO_2^-, with $\delta^{15}N$ value similar to NO_2^- in TSP. This isotopic similarity suggests that wind-blown soil is probably the primary source of NO_2^- in TSP, accounting for the background levels. While concentration changes of water-soluble inorganic ions in TSP and $PM_{2.5}$ in response to shifts in air mass back-trajectories imply that atmospheric pollutants transported from South Asia may further elevate the NO_2^-, the specific mechanisms of long-range transport resulting in NO_2^- accumulation in TSP rather than $PM_{2.5}$ remain unknown and need to be investigated. The elevated levels of TSP NO_2^- may readily participate in atmospheric reactive nitrogen cycling through gas-particle partitioning or photolysis, leading to the production of HONO, OH and NO and thereby influencing oxidation chemistry. Further efforts on the sources and atmospheric chemistry of particulate nitrite are warranted, particularly in the pristine Tibetan Plateau, where even small inputs of NO_x or HONO can disproportionately affect oxidant budgets and reactive nitrogen cycling.

1 Introduction

The Himalayas-Tibetan Plateau (HTP) represents one of the most important geomorphologically cryospheric regions, boasting high abundance of alpine glaciers and extensive areas of high-altitude snow cover (Kehrwald et al., 2008; Yao et al., 2012; Kang et al., 2019). The melting of snow cover and glacier ice holds immense importance as crucial freshwater resources for over 1.4 billion people in Asia, earning HTP the title as the "Water Tower of Asia" (Immerzeel et al., 2010). However, the enhanced warming rate in the Tibetan Plateau (TP, ~ 0.30°C per decade) has resulted in a rapid and alarming increase in glacier melting over the past decade, significantly affecting the climate, hydrological cycles, and ecosystems at local and global scales (Immerzeel et

50 ~~al., 2010; Xu et al., 2009; Lau et al., 2010). Persistently increased aerosol loadings and greenhouse~~

51 ~~gas in TP region account for the increased warming rate (Kang et al., 2019; Lau et al., 2010; Lüthi~~

52 ~~et al., 2015). More importantly, once deposited on the surface of snow cover and glacier ice, the~~

53 ~~aerosol, especially these light-absorbing components (i.e., black carbon, dust) contribute~~

54 ~~significantly to the rapid glacial retreat (Xu et al., 2009; Zhao et al., 2020).~~

55 The Tibetan Plateau (TP), known as the "Third Pole", represents one of the most climate-

56 sensitive regions on Earth (Yao et al., 2012). Over recent decades, the TP has experienced significant

57 and rapid climate warming, primarily driven by increasing aerosol loadings and greenhouse gas

58 concentrations due to its geographic proximity to East and South Asia with intensive anthropogenic

59 emissions (Kang et al., 2019; Lau et al., 2010; Lüthi et al., 2015). Atmospheric oxidation capacity

60 (AOC) regulates secondary aerosol formation and trace gases removal, including CH_4 (Wang et al.,

61 2023; Ye et al., 2023; Ye et al., 2016; Andersen et al., 2023), therefore acting as a critical link

62 between atmospheric pollution and ~~cryospheric~~ regional climate warming~~changes~~. Previous ~~study~~

63 studies have suggested strong solar radiation, high ozone (O_3) and relatively high water vapor

64 dominate the relatively strong AOC over the TP (Lin et al., 2008). Recent field campaign further

65 highlighted the rapid reactive nitrogen cycling, with N(III) species (i.e., HONO) as the intermediate,

66 also plays an important role in maintaining the strong AOC in TP (Wang et al., 2023). For example,

67 *Wang et al.* reported high-than-expected HONO (~30 ± 13 pptv) in the Namco station, a ~~typical~~

68 representative background site in the middle of TP, with HONO sources including NO_2

69 heterogenous conversion, soil emission and particulate nitrate photolysis (Wang et al., 2023).

70 Incorporating the observed HONO into model simulations approximately doubled the estiamted OH

71 abundance compared to simulations without HONO constraints. However, a detailed HONO budget

72 analysis indicated these three dominant sources could not account for the observed daytime HONO

73 levels at the background site, implying the existence of additional, yet unidentified, HONO sources.

74 Particulate nitrite (NO_2^-) likely represents a potential source of HONO through thermodynamic

75 partitioning processes under favorable atmospheric conditions, provided particulate nitrite is present

76 in significant amounts (Vandenboer et al., 2014a; Chen et al., 2019; Li, 1994). Interestingly,

77 relatively high levels of nitrite in total suspended particulate (TSP) have also been reported from

78 remote sites of TP, i.e., in a forest site in the Southeast Tibet (~ 140 ng m^{-3}) and at the Qomolangma

79 monitoring station (QOMS, ~ 60 ng m^{-3}) (Bhattarai et al., 2019; Bhattarai et al., 2023). Such high

80 levels of particulate NO$_2^-$ may also contribute to the strong AOC in TP, either via directly photolysis

81 to produce NO$_x$ (Jacobi et al., 2014) or indirectly serve as an important source of HONO through

82 gas-particle partitioning (R1). However, the sources and formation mechanisms for the relatively

83 high level of atmospheric NO$_2^-$ observed in the TP remain unclear.

84 $$\text{HONO}_{(g)} \leftrightarrow \text{HONO}_{(aq)} \leftrightarrow \text{NO}_2^-{}_{(aq)} + \text{H}^+{}_{(aq)} \text{ (R1)}$$

85 $$\cancel{\text{HONO}_{(aq)} + \text{H}^+{}_{(aq)} \leftrightarrow \text{H}_2\text{ONO}^+{}_{(aq)} \text{ (R2)}}$$

86 $$\cancel{\text{HONO} + h\upsilon \text{ (300 nm} < \lambda < \text{405 nm)} \rightarrow \text{NO} + \text{OH (R3)}}$$
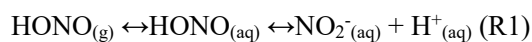
87 The stable nitrogen and oxygen isotopic compositions (δ^{15}N, δ^{18}O, and $\varDelta^{17}$O; where $\delta =$

88 $(R_{sample}/R_{reference} - 1) \times 1000‰$ and with R denoting the ^{15}N/^{14}N, ^{18}O/^{16}O, and ^{17}O/^{16}O ratios; $\varDelta^{17}$O $=$

89 δ^{17}O $- 0.52 \times \delta^{18}$O) may provide diagnostic information regarding the sources and formation

90 pathways of atmospheric nitrite. Similar isotopic approaches have been widely used to explore the

91 nitrate (NO$_3^-$) sources (Morin et al., 2008; Zong et al., 2020; Geng et al., 2014; Fang et al., 2011;

92 Hastings et al., 2003; Zhang et al., 2022; Zhang et al., 2021b; Liu et al., 2018; Felix and Elliott,

93 2014; Miller et al., 2018). Considering that atmospheric NO$_2^-$ may share similar sources and

94 formation pathways with NO$_3^-$, the specific NO$_2^-$ formation pathways are expected to be

95 characterized by distinct oxygen or nitrogen isotopic endmembers, despite reports on the

96 atmospheric NO$_2^-$ isotopic compositions are rare. For instance, NO$_2^-$ produced from the photolysis

97 of particulate NO$_3^-$ may possess very negative δ^{15}N values compared to NO$_3^-$, analogous to the

98 pronounced nitrogen isotope fractionation effects associated with snow nitrate photolysis (Erbland

99 et al., 2013; Frey et al., 2009), while the $\varDelta^{17}$O of NO$_2^-$ is expected to closely resemble that of NO$_3^-$

100 as the oxygen atom in NO$_2^-$ is imparted from NO$_3^-$, unless significant oxygen atom exchange

101 between NO$_2^-$ and aerosol water occurs. The $\varDelta^{17}$O of NO$_2^-$ (and HONO) from primary emission

102 sources is expected to be negligible, while that generated from heterogeneous reactions of NO$_2$ on

103 the aerosol surface would be characterized by positive $\varDelta^{17}$O values depending on the degree of NO$_2^-$

104 and aerosol water oxygen isotope exchange. These unique isotopic fingerprints may be utilized in

105 distinguishing the sources and formation pathways of atmospheric NO$_2^-$.

106 To gain insight into the sources and/or formation mechanisms of atmospheric NO$_2^-$ in the pristine

environment of TP, we collected the TSP and fine particulate matter ($PM_{2.5}$) synchronously at the Base Camp, the north slope of the Mt. Qomolangma during the campaign of "Earth Summit Mission-2022" scientific expedition from April 24th to May 6th, 2022, with additional surface soil samples collected in May, 2023. The NO_2^- concentration and multi-isotopic signatures ($\delta^{15}N$, $\delta^{18}O$, and $\Delta^{17}O$) in aerosol and surface soil were then determined in order to evaluate the potential sources of atmospheric NO_2^-. Additionally, the potential environmental implication of atmospheric nitrite was explored in the term of atmospheric oxidation capacity at this pristine environment.

2 Material and Method

2.1 Site description

The Base Camp is located in the middle of the Rongbuk valley (86.85 °E, 28.14 °N), situated ~5200 m above sea level (m a.s.l) on the north slope of the Mt. Qomolangma (Zou et al., 2008; Zhu et al., 2006). The surrounding surface consists of loosed soil, gravel, broken rocks of various sizes, with sparse vegetation due to the semi-arid status (Ming et al., 2007; Zou et al., 2008). Rongbuk valley is characterized by a depth of ~1000 m and a floor width of ~1000 m, with elevations of the surrounding mountains exceeding 6000 m on both sides (Zou et al., 2008). Attributed to the unique topography, the local air circulation is dominated by mountain and valley breezes. The predominant wind regime is the katabatic flow of southerly and southeasterly, which is typically persists from noon to midnight (Zhu et al., 2006; Zou et al., 2008; Zhou et al., 2011). The nearest accessible area for residents and visitors is at least 2 km north of the Base Camp. During the campaign, electricity and natural gases were routinely used for cooking and hot water production. There were intermittent vehicle exhaust emissions around the station during daytime for the daily necessaries supporting, i.e., water and food. To minimize the influence of local anthropogenic activities on sampling, the instruments were set in the southeast (upwind direction, Figure S1) and approximately 100 m away from the living space of the Base Camp. The anthropogenic influence on the sampling is expected to be minimal.

2.2 Field campaign and sample collection

From April 26th to May 6th, 2022, TSP samples were collected simultaneously with NO_2 using a homemade denuder-filter system (Zhou et al., 2022). A similar system has been widely used to

135 separately collect atmospheric particulate matter and N-containing gases for isotopic analysis (Chai

136 et al., 2019; Chai et al., 2021), suggesting the mutual interference between the particulate and

137 gaseous phases to be minimal. A polytetrafluoroethylene (PTFE) sleeve is used to assemble the

138 homemade denuder with the filter pack, flowmeter, and pump. The filter pack was placed in the

139 front of the denuder. All connections between the various parts of the sampling apparatus are made

140 using 3/8″ Teflon tubing. A detailed description of the sampling apparatus can be found in our

141 previous report (Zhou et al., 2022). Whatman quartz filter (circles, diam. 47mm, pre-heated at 400 ℃

142 for 3 h before use) was placed into the filter pack to collect TSP sample. In the present study, the

143 collected bulk aerosol can be regarded as TSP since no size-selective inlet was employed. The flow

144 rate was controlled at 30 Lmin^{-1} using a flowmeter. Previous reports have indicated that the flow

145 rate has negligible effect on the concentrations of sulphate, nitrate, and ammonium when using

146 quartz filter for sampling (Keck and Wittmaack, 2005). To minimize the potential influence of the

147 loose ground surface on the TSP collection, a mountain tent was used to separate the pump (out the

148 tent) with the denuder-filter system (in the other side of tent), and the inlet Teflon tube was stretched

149 out of the tent for ~1.5 m height straight.

150   From April 24th to May 6th, 2022, PM$_{2.5}$ were sampled using a high-volume aerosol sampler

151 (TH-1000F; Wuhan Tianhong Instruments Co. Ltd., China) equipped with PM$_{2.5}$ inlet and Whatman

152 quartz-fiber filters (sheets, 203 mm × 254 mm) at a flow rate of 1.5 m^3/min. All the quartz filters

153 were pre-heated at 400 ℃ for 3 h before use. In general, TSP and PM$_{2.5}$ samples were collected with

154 diurnal resolution during this campaign, with daytime samples from approximately 09:00–20:00

155 and nighttime samples from 21:00–08:00 (local time), respectively. From May 2nd to May 4th, we

156 collected the daytime TSP and PM$_{2.5}$ samples in the morning (09:00-14:00) and afternoon (14:00-

157 20:00), respectively. A total of 24 TSP samples (including 2 blanks) and 29 PM$_{2.5}$ (including 3 blanks)

158 were collected during this campaign. After each sampling period, quartz filters were removed from

159 the filter pack/PM$_{2.5}$ inlet and immediately wrapped in pre-baked aluminum foil and then stored in

160 frozen until analysis to minimize potential loss of nitrite. During the campaign, snowfall events

161 occurred on the night of April 29th and during the daytime of April 30th.

162   Surface soil samples (0-5 cm depth, n = 9) were collected in May, 2023 from the east slope,

163 west slope and south sides of the Rongbuk valley. A polytetrafluoroethylene (PTFE) shovel was

164 used to collect soil. The collected soil was immediately transferred to clean plastic bags, sealed and

165 kept frozen. Soil samples were transported into laboratory using a cold chain. Upon arrival at our

166 laboratory, the soil samples were passed through a 60-mesh screen (~0.25 mm) to remove larger

167 particles and thoroughly homogenized prior to chemical and isotopic analysis.

2.3 Ionic concentration analysis and uncertainty estimation

169 Water-soluble inorganic ions (WSIs, including Na^+, NH_4^+, K^+, Mg^{2+}, Ca^{2+}, Cl^-, NO_2^-, NO_3^-, and

170 SO_4^{2-}) in TSP (entire filter, ~16.6 cm^2) and $PM_{2.5}$ (1/32 section, ~13.0 cm^2) were extracted using 20

171 mL Milli-Q ultrapure water (18.2Ω cm) in an ultrasonic bath at room temperature for 30 min. Note

172 the TSP filters were cut to fit the filter holder from the standard Whatman quartz-fiber filters which

173 were also used as the $PM_{2.5}$ filters. After filtration through a 0.22 μm pore size syringe filter which

174 was pre-cleaned with ultrapure water, the filtrate was subjected to inorganic species analysis using

175 ion chromatography (Dionex Aquion) (Zhang et al., 2020). Blank filters were pretreated and

176 measured the same as real samples, and the limits of detection (LOD) was calculated as 3 times of

177 standard deviations of blanks (Fang et al., 2015a). In general, Na^+ in the blank filters is comparable

178 to samples, a well-known issue for the Whatman quartz filter which is high in Na^+ blank. Therefore,

179 in this study, we discarded the Na^+ data. The volatile components (i.e., NH_4^+, NO_2^-, NO_3^-) and K^+

180 in blank are low but several times higher than the detection limits; SO_4^{2-}, Mg^{2+} and Ca^{2+} in blank

181 are significantly higher than the respective LOD but lower than samples by at least five times (the

182 lower end). All reported concentrations of each ion were blank corrected as follows:

183
$$C_i = \frac{(\rho_{sample} - \rho_{blank}) \times V_{water} \times F}{V_{air}}$$

184 with C_i representing the ambient concentrations of specie i in air (ng m^{-3} or μg m^{-3}), ρ_{sample} and

185 ρ_{blank} are the concentrations determined by the ion chromatography (ng mL^{-1}), V_{water} is the volume

186 of ultrapure water used for extraction (20 mL), V_{air} is the volume of air sampled for each $PM_{2.5}$ or

187 TSP filter, F is the ratio of particulate matter collection area for $PM_{2.5}$ or TSP filters to the filter area

188 used for extraction.

189 The overall uncertainty in ion concentration was estimated according to the law of error

190 propagation, accounting for the sampling air volume (3% for $PM_{2.5}$ samples and 1% for TSP samples

191 as provided by the manufactures), the extraction of water volume (~0.3% for pipetting from the

192 manufacture Eppendorf), the blanks, and the analytical uncertainty from ion chromatography and

193 calibration, assuming that these factors are independent. The analytical uncertainty for water-soluble

194 ions concentration determination using ionic chromatography has been extensively assessed in our

195 laboratory, with values typically <5% for all inorganic species at concentration of 500 ng mL^{-1}. The

196 combined uncertainty about the ionic concentrations in PM$_{2.5}$ and TSP are shown in Table S1. In

197 general, TSP samples are associated with relatively high overall uncertainty compared to PM$_{2.5}$

198 samples, perhaps due to the relatively high blank variability due to the low mass loading in TSP.

199 For soil ionic concentration analysis, 4.0 g sieved soil was extracted using 20 mL Milli-Q

200 ultrapure water, shaken for 30min at room temperature. After centrifugation, the extract was passed

201 through 0.45 mm filters before ions analysis. The concentration determination of water-soluble

202 inorganic ions in soil extract was similar to that of aerosol samples. Detailed procedure for the

203 extraction of soil inorganic ions, especially the NO$_2^-$ has been descried in previous report (Homyak

204 et al., 2015).

2.4 Isotopic analysis

206 After concentration measurements, isotopic analyses (δ^{15}N, δ^{18}O, and Δ^{17}O) of NO$_2^-$ in TSP

207 were conducted using the azide method (Casciotti et al., 2007). The azide method can reduce nitrite

208 ion in solution into N$_2$O in a single step, while nitrate ion remains unchanged, ensuring no

209 interference on the nitrite isotopic analysis. The azide reagent is prepared by mixing 2 M sodium

210 azide with 40% acetic acid at a 1:1 ratio by volume in our laboratory. NO$_2^-$ standards and samples

211 were pretreated under identical conditions concerning the total volume, nitrite amount, water isotope,

212 and matrix. The δ^{15}N, δ^{18}O, and δ^{17}O of N$_2$O reduced from NO$_2^-$ in the TSP samples and standards

213 were determined using a Finnigan$^®$ MAT253 plus isotope ratio mass spectrometer (IRMS) equipped

214 with a GasBench II and preconcentration system. The data calibration followed the procedures

215 described in *Albertin et al*., 2021, using three international KNO$_2$ salt standards (RSIL-N10219,

216 RSIL-N7373, and RSIL-N23 with respective δ^{15}N and δ^{18}O values of 2.8/88.5 ‰, -79.6/4.2 ‰, and

217 3.7/11.4‰). The Δ^{17}O values of the three international references have not been certified. To address

218 this, a series laboratory experiments was conducted to determine the true values of three

219 international references in our laboratory (Zhang et al., 2025). In brief, each nitrite international

reference was oxidized into NO_3^- by O_3 produced from commercial ozone generator. A parallel flow of O_3 was also used to convert a normal KNO_2 salt ($\Delta^{17}O = 0$) into NO_3^- to quantify the $\Delta^{17}O$ transfer during O_3 oxidation, following the approach of (Vicars and Savarino, 2014). Based on these experiments, the $\Delta^{17}O$ of RSIL-N7373 and RSIL-N23 are determined to be negligible, consistent with previous findings (Albertin et al., 2021), while the $\Delta^{17}O$ of RSIL-N10219 is determined to be (-9.3 ± 0.2) ‰ in our laboratory. The ^{17}O-excess in samples is then calculated as $\Delta^{17}O = \delta^{18}O - 0.52 \times \delta^{17}O$. The standard deviations for $\delta^{15}N$, $\delta^{18}O$, $\Delta^{17}O$ of reference materials (n = 10) were determined to be less than 0.1‰, 0.6‰, and 0.4‰, respectively.

For soil NO_2^- isotopic analysis, ~30.0g sieved soil was extracted using 150 mL Milli-Q purewater. The soil extract was then preconcentrated into 10 mL using ion-exchange resin before isotopic analysis. The preconcentration approach was widely used for nitrate isotopic analysis in snow and ice samples, and the detailed procedures and the performance have been provided in *Erbland et al.,* 2013 and evaluated in our laboratory (Text S1). The concentrated soil extracts (50 nmol NO_2^-) was then subjected to soil NO_2^- isotopic analysis by converting into N_2O via the azide method. For soil NO_3^- isotopic analysis, ~5.0g sieved soil was extracted with 15 mL of 2M KCl solution (Fang et al., 2015b). The remaining procedures of soil NO_3^- and NO_2^- analysis were same as those for TSP samples, as aforementioned.

2.5 Complementary analyses of air mass backward trajectory

To evaluate the possible impact of biomass burning emissions or other pollution sources from South Asia, the Hybrid Single-Particle Lagrangian Integrated Trajectory (HYSPLIT) model (performed using TrajStat plugin of the MeteoInfo software) and archived Global Data Assimilation System (GDAS) of meteorological data were used to model the air mass back trajectories (Wang, 2014). In this study, 3-day air mass backward trajectories with arriving height of 1000 m above ground level were simulated to identify the most likely pathway and potential source regions of the air masses at the Base Camp (Bhattarai et al., 2023; Lin et al., 2021). Moreover, the Fire Information and Resource Management System (FIRMS) developed by Moderate Resolution Imaging Spectrometer (MODIS) (https://worldview.earthdata.nasa.gov) was employed to identify the distribution of active fire spots during the sampling period.

3 Results

3.1 Mass concentrations of water-soluble inorganic ions in TSP and PM$_{2.5}$

Figure 1 displays the chemical compositions of water-soluble inorganic ions, their corresponding time series and fractional contributions in TSP and PM$_{2.5}$. Throughout the campaign, substantial variations of total WSIs in PM$_{2.5}$ and TSP were observed. For PM$_{2.5}$ samples, the mass concentrations of total WSIs before April 30th were higher than that from May 1st to May 6th (4.1 ± 1.7 versus 1.7 ± 0.6 μg m^{-3}; $p < 0.05$). The cut-off date of April 30th was selected based on observed shifts in concentrations of water-soluble ions and air mass origins (described in section 4.2). This decline of total WSIs after April 30th was predominately driven by significant reductions in secondary inorganic species, i.e., SO$_4^{2-}$, NO$_3^-$ and NH$_4^+$, with the magnitude by more than 60%. In particular, NH$_4^+$ in PM$_{2.5}$ was on average (322 ± 243) ng m^{-3} before April 30th whereas NH$_4^+$ in PM$_{2.5}$ collected during daytime and nighttime of May 1st were 1 ng m^{-3} and 3 ng m^{-3}, respectively, and NH$_4^+$ in PM$_{2.5}$ extractions from May 2nd to May 6th was below the detection limit. Therefore, the fractional contribution of secondary inorganic species in PM$_{2.5}$ also decreased (Figure 1d). Similarly, K$^+$ in PM$_{2.5}$, a good tracer of biomass burning (Ma et al., 2003), also declined significantly after April 30th (269 ± 432 versus 22 ± 12 ng m^{-3}; $p < 0.05$). The elevated concentrations of WSIs before April 30th (4.1 ± 1.7 μg m^{-3}) are comparable to previous reports at QOMS station (4.2 ± 2.2 μg m^{-3}) in the spring (Lin et al., 2021). In comparison, concentrations of Ca^{2+} and Mg^{2+}, tracers of wind-blown dust (Wang et al., 2002), decreased by less than 20% after April 30th. In general, SO$_4^{2-}$, NO$_3^-$, and Ca^{2+} are the most abundant species in PM$_{2.5}$, accounting for the majority of the mass of total WSIs. In addition, no clear diurnal variation of water-soluble inorganic ions in PM$_{2.5}$ was observed in this study (Figure S2).

270
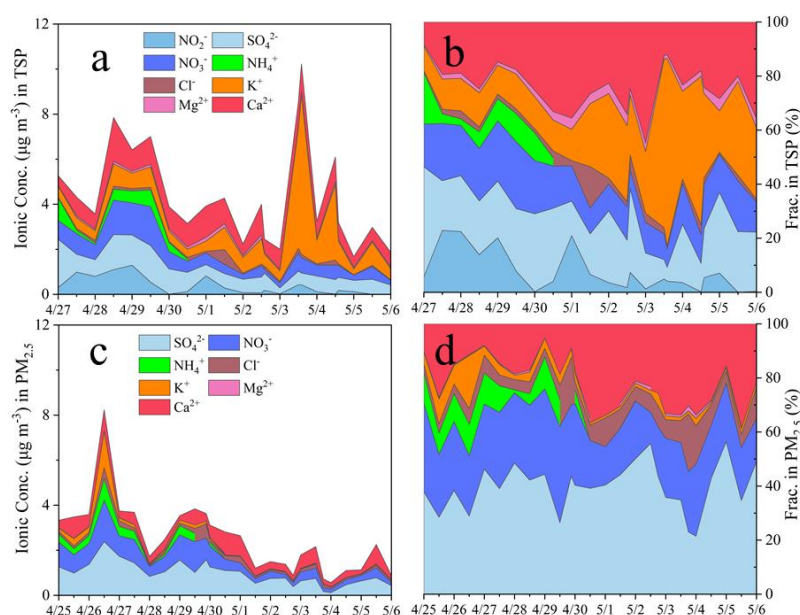
Figure 1. The chemical compositions and time series of mass concentrations of water-soluble inorganic species (NO_2^-, SO_4^{2-}, NO_3^-, Ca^{2+}, etc.), as well as the corresponding mass fractions in respective TSP (a, b) and $PM_{2.5}$ (c, d) samples collected at Base Camp of Mt. Qomolangma in spring 2022.

275
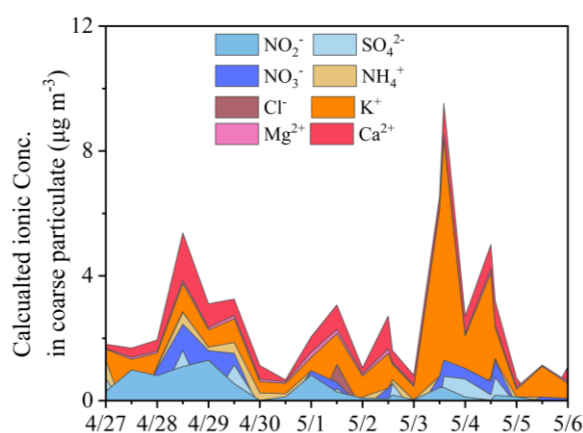
Figure 2. The estimated chemical compositions and time series of mass concentrations of chemical species (NO_2^-, SO_4^{2-}, NO_3^-, Ca^{2+}, etc.) in coarse-mode particulate during the springtime campaign (calculated as the difference between TSP and $PM_{2.5}$). Discontinuities in the time series were observed for certain species (e.g., SO_4^{2-}), likely resulting from relatively lower concentrations in the TSP samples compared to those in the corresponding $PM_{2.5}$ samples. This discrepancy is likely attributed to the propagated uncertainties involved in the concentration analysis, sampling approach and blank corrections.

Some water-soluble inorganic ions (e.g., SO_4^{2-}, NO_3^- and NH_4^+) in TSP showed similar variation trends with that in $PM_{2.5}$ throughout the campaign, while others, such as K^+, exhibited

285   divergent behavior (Figure 1). For example, after April 30th, the secondary inorganic species in TSP

286   declined considerably by over 50% (i.e., NH_4^+ in TSP declined by more than tenfold), while Ca^{2+} in

287   TSP decreased with a smaller degree (< 15%) and Mg^{2+} remained stable. In contrast, TSP K^+ (from

288   both crustal and biomass burning sources)(Hsu et al., 2009) drastically surged on May 3rd and May

289   4th. Note that other species in TSP, i.e., SO_4^{2-} and NO_3^- also increased to some extent on May 3rd.

290   The time series of water-soluble inorganic ions in the coarse-mode particulate, calculated as the

291   differences between TSP and $PM_{2.5}$, are presented in Figure 2. Due to the overall analytical

292   uncertainties, the air concentrations of SO_4^{2-} in $PM_{2.5}$ samples occasionally exceeded that in

293   corresponding TSP samples on some days.

294   Figure 3 presents the ion balance of measured water-soluble ions in $PM_{2.5}$ throughout the

295   campaign as well as in TSP collected before and after April 30th, respectively, to highlight the

296   significant decline in TSP NO_2^-. There is a strong correlation between cation and anion equivalents

297   in $PM_{2.5}$ samples ($R^2 = 0.70$), whereas the correlations decreased in TSP samples ($R^2 = 0.46$ before

298   April 30th and 0.49 after that, respectively). The nanogram-equivalent weight of cation were

299   significantly higher than that of anions for all samples, with ratio of cation to anion equivalent of ~

300   1.5 for $PM_{2.5}$, ~1.9 for TSP collected before April 30th, ~4.2 for TSP collected after May 1st. Clearly,

301   the declines in TSP NO_2^- after April 30th resulted in relatively higher cation/anion equivalent ratio.

302   The slopes of the correlation lines exceeded unity for $PM_{2.5}$ and TSP samples, indicating the alkaline

303   nature of aerosol. The observed deficiency of anion can be attributed to the presence of carbonates

304   (i.e., $CaCO_3$), which can dissolve in water during extraction to release CO_3^{2-} and/or HCO_3^- despite

305   the relatively low solubility (Zhang et al., 2021a).

306   The most distinct feature of chemical compositions in TSP was the elevated level and

307   significant variation of NO_2^-, ranging from 0.2 ng m^{-3} to 1291 ng m^{-3} in air and with an average of

308   375 ± 386 ng m^{-3}. In comparison, NO_2^- consistently remained below the detection limit in $PM_{2.5}$

309   samples. Note during the laboratory measurements of ionic concentrations, TSP and $PM_{2.5}$ filters

310   were extracted with ultrapure water and it was the extraction analyzed by ion chromatography. To

311   ensure fair comparisons, similar areas of filters were extracted with same volume of ultrapure water,

312   so that the extractions from the $PM_{2.5}$ filters should be more concentrated in atmospheric particulate

313   species compared to that from the TSP filters, since $PM_{2.5}$ samples were collected at a much faster

sampling speed (1.5 m³ min⁻¹ vs. 30 L min⁻¹) over the same sampling duration. Nevertheless, NO_2^- was detectable only in the extractions of TSP filter. The determined NO_2^- concentrations in TSP in this study (375 ± 386 ng m⁻³) were higher than previous reports conducted in various remote sites, such as at QOMS station (~60 ng m⁻³ for TSP) (Bhattarai et al., 2023), at a forest site in the Southeast Tibet Plateau (~140 ng m⁻³ for TSP) (Bhattarai et al., 2019), in the middle hills of the central Himalayas (~210 ng m⁻³ for TSP) (Tripathee et al., 2021).

In particular, there was a dramatic decrease in TSP NO_2^- after April 30th, from a mean of (625 ± 457) ng m⁻³ to (147 ± 145) ng m⁻³, in line with the declines in other secondary inorganic species. Over the course of the campaign, NO_2^- comprised approximately 8% of the total WSIs mass in TSP, while its contribution reached maximum of ~20% on April 27th and April 28th, being one of the most abundant components on the two days. In addition, there was a strong correlation between NO_2^- and NO_3^- throughout the campaign ($r = 0.75$, $p < 0.05$. Figure S3). Meanwhile, the mean mass ratio of NO_2^- to NO_3^- was ~50% throughout the campaign, but on several days (i.e., night of April 27th) NO_2^- concentrations significantly exceeded that of NO_3^- (802 vs. 663 ng m⁻³). Previous study also reported comparable NO_2^- and NO_3^- concentrations in at a forest site in the Southeast Tibet (summer:100 ng m⁻³ vs. 110 ng m⁻³; winter: 180 ng m⁻³ vs. 270 ng m⁻³) (Bhattarai et al., 2019).
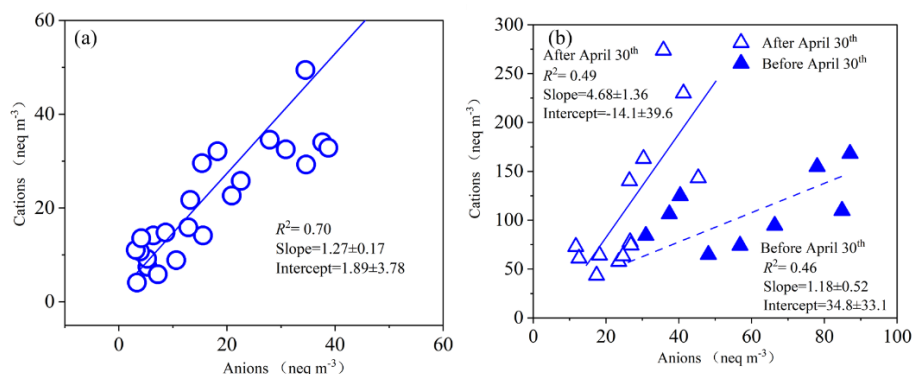
Figure 3. Ion balance for PM₂.₅ (a, blue circles) and TSP samples (b, blue hollow triangles: samples collected after April 30th; blue solid triangles: samples collected before April 30th). Concentrations are expressed in nanogram-equivalent weight per cubic meter (neq m⁻³).

3.2 Isotopic signatures of nitrite in TSP

Figure 4 presents the times series of $\delta^{15}N$, $\delta^{18}O$ and $\Delta^{17}O$ of NO_2^- in TSP, along with the NO_2^-

336 concentrations. Similar to the variation trend of NO_2^- concentrations, NO_2^- isotopes varied in a wider

337 range before April 30th, but became more stable afterward. For example, $\delta^{15}N(NO_2^-)$ ranged from -

338 10.9 ‰ to 0.8 ‰, with a relatively large standard deviation before April 30th compared to that after

339 May 1st ((-6.4 ± 4.3) ‰ vs. (-8.0 ± 0.7) ‰). The large variability in $\delta^{15}N(NO_2^-)$ before May 1st is

340 predominately attributed to the two high values observed in daytime of April 27th and night of April

341 28th. Note that the two high $\delta^{15}N(NO_2^-)$ samples were also associated with relatively high NO_2^- mass

342 concentrations. In contrast to the declining trend of NO_2^- concentrations, the mean $\delta^{15}N(NO_2^-)$

343 values were comparable before and after April 30th. Relatively large variability was observed in TSP

344 $\delta^{18}O(NO_2^-)$, ranging from -9.0‰ to 3.9‰ and with an average of (-3.4 ± 3.8) ‰. TSP $\Delta^{17}O(NO_2^-)$

345 varied within a narrow range from -0.2‰ to +0.7‰ and with a mean of (0.2 ± 0.3) ‰. During the

346 campaign, no significant correlations were observed between $\delta^{15}N(NO_2^-)$ and the NO_2^-

347 concentrations; while $\delta^{18}O(NO_2^-)$ appeared to be moderately correlated with the NO_2^-

348 concentrations (Figure S5).

349
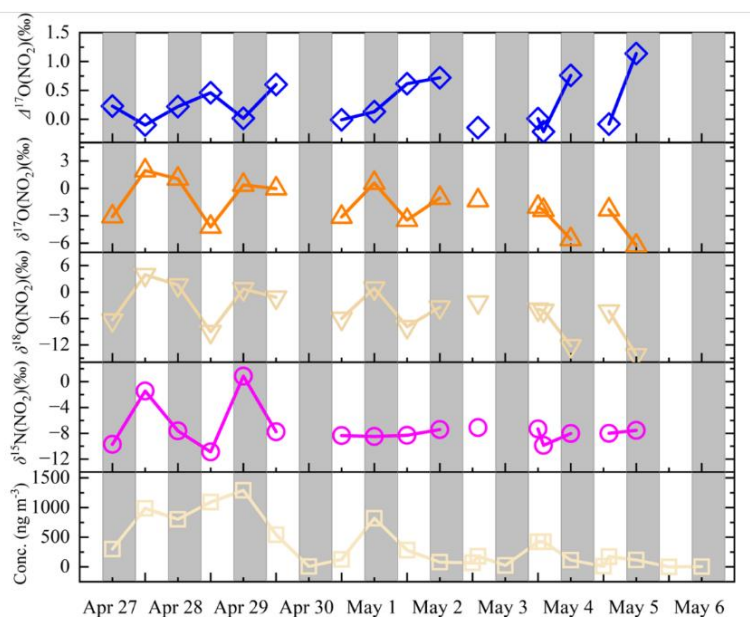
350 **Figure 4.** Time series of multiple isotopic signatures of NO_2^- ($\delta^{15}N$, $\delta^{18}O$, $\delta^{17}O$ and $\Delta^{17}O$) as well as

351 corresponding concentrations in TSP samples during "Earth Summit Mission" scientific expedition

352 in spring 2022. The gray shaded area denotes local nighttime.

353 **Table 1.** The measured nitrite (and nitrate) concentration and isotopic signatures in surface soil
354 collected in the Rongbuk Valley.

Soil sample ID	NO_2^-	NO_3^-

	Conc.(ng g^{-1})	δ^{15}N	δ^{18}O	Δ^{17}O	Conc.(ng g^{-1})	δ^{15}N	δ^{18}O	Δ^{17}O
East-1	67.7	-12.0	6.1	3.3	1127.3	-2.7	23.4	5.7
East-2	76.1	-11.9	2.7	2.2	1098.3	1.3	18.1	3.8
East-3	82.3	-14.6	6.0	3.3	2978.1	-0.3	25.4	6.6
West-1	88.6	-10.1	8.9	1.6	3176.5	-3.1	44.5	13.4
West-2	106.2	-7.0	11.4	1.5	2880.3	-1.2	22.1	6.2
West-3	179.3	-5.2	12.7	1.4	7686.9	-3.4	35.8	11.4
South-1	53.8	-13.2	12.7	6.7	3651.2	-0.6	32.6	10.1
South-2	42.3	-9.0	18.1	7.3	1683.2	-2.2	49.3	14.8
South-3	48.9	-10.3	12.4	6.7	385.5	-2.4	45.7	14.9

355

3.3 Surface soil nitrite concentration and isotopic signature

The concentration of soil NO_2^- (and NO_3^-) as well as the corresponding isotopic signatures are displayed in Table 1. The soil NO_2^- content on the west slope of Rongbuk Valley (on average 124.7 ng g^{-1}) was higher than that observed on the east and south sides (75.3 ng g^{-1} and 48.3 ng g^{-1}, respectively). The mean surface soil NO_2^- and NO_3^- in the Rongbuk Valley were 82.8 and 2740.8 ng g^{-1}, respectively. The soil NO_3^- concentrations were significantly higher than the NO_2^- by a factor of 8 ~ 40. In general, the measured soil NO_3^- concentrations at the Rongbuk valley were significantly lower than other remote regions of TP (i.e., 23.1 μg g^{-1} at Naqu, 8.4μg g^{-1} at Yangbajing), while soil NO_2^- concentrations were comparable to these reports (i.e., 90.3 ng g^{-1} at Naqu,131.2 ng g^{-1} at Yangbajing) (Wang et al., 2019). Soil δ^{15}N(NO_2^-) values ranged from -13.2‰ to -5.2‰ (on average -10.4‰), which are comparable to TSP δ^{15}N(NO_2^-) (-7.3‰). In comparison, we observed positive soil δ^{18}O(NO_2^-) and Δ^{17}O(NO_2^-), ranging from 2.7‰ to 18.1‰ (on average 10.5‰) and 1.4‰ to 7.3‰ (on average 3.8‰), respectively, in contrast to the negative δ^{18}O(NO_2^-) and near-zero Δ^{17}O(NO_2^-) observed in TSP samples. The determined soil δ^{18}O(NO_2^-) is comparable to that in laboratory incubated soil (11.8‰ ~ 12.5‰) (Lewicka-Szczebak et al., 2021).

4 Discussion

The significant contrast in NO_2^- concentrations between TSP and PM$_{2.5}$ samples, as shown in Figure 1, suggests that at the sampling site atmospheric particle NO_2^- overwhelmingly exists in coarse particles. This observation is consistent with previous studies across the TP, which also reported the absence of NO_2^- in fine mode particles (PM$_{2.5}$ and PM$_{1.0}$) using either online real-time instrument or offline filter sampling (Decesari et al., 2010; Xu et al., 2020; Xu et al., 2023; Zhao et al., 2020), while relatively high levels of TSP NO_2^- have been reported (Bhattarai et al., 2019;

378   Bhattarai et al., 2023; Tripathee et al., 2017). In general, the chemical sources of particle NO_2^- in

379   the atmosphere encompass the uptake of HONO, particulate nitrate photolysis, and the NO_2-related

380   reactions (i.e., photo-enhanced uptake of NO_2 on mineral dust, heterogeneous reaction of NO_2 on

381   the surface of aerosol) (Nie et al., 2012; Vandenboer et al., 2014a; Chen et al., 2019; Shang et al.,

382   2021), as summarized in Table 2. In addition to these in-situ atmospheric processes, growing

383   evidence has revealed that long-range transport of atmospheric pollutants from South Asia also

384   contributes considerably to aerosol loadings in TP in the spring (Kang et al., 2019; Bhattarai et al.,

385   2023; Zhao et al., 2020), which may also bring nitrite along with other pollutants. Moreover, the

386   lifting of surface dust can also contribute to the atmospheric coarse particles and significantly

387   influence the chemical composition of TSP (Zhang et al., 2021a; Pokharel et al., 2019), and therefore

388   soil nitrite could also be a potential source for TSP NO_2^-. In the following discussion, we examine

389   the potential importance of the abovementioned processes to the observed high NO_2^- content in

390   coarse particle and discern the most likely ones.

391   **Table 2.** Particulate nitrite concentration and formation pathways/sources compiled in the literature.
392

Site	Period	NO_2^- Conc. (mean, ng m^{-3})	Formation pathways/Sources	Reference
QOMS station	April 2017	60	Biomass burning emission transported from South Asia	Bhattarai et al., 2023
Bakersfield, California	May–July 2010	150	HONO uptake on lofted alkaline soil particles.	VandenBoer et al., 2014
Jinan, China	November 2013 − January 2014	2080	Heterogeneous reactions of NO_2	Wang et al., 2015
Seoul, Korea	May−July, 2005	1410	Heterogeneous reactions of NO_2	Song et al., 2009
Shanghai, China	June 2020	210	Heterogeneous reactions of NO_2, reduction of NO_2 by S(IV)	Shang et al., 2021
Mt.Heng, China	April 2009	2500	Surface TiO_2 photocatalysis of NO_2	Nie et al., 2012

393   **4.1 The potential effects of atmospheric chemistry on NO_2^- in TSP**

394   Increasing evidence supports particulate nitrate photolysis as an important source of

395   atmospheric HONO especially in pristine atmosphere, with NO_2^- serving as the intermediate in the

396   subsequent gas-particle partition process (Andersen et al., 2023; Ye et al., 2016). In theory,

397   particulate NO_2^- (and HONO) produced from particulate nitrate photolysis might be associated with

398   extremely negative $\delta^{15}N$ values, due to the significant nitrogen isotopic fractionation effect during

nitrate photolysis (Erbland et al., 2013; Frey et al., 2009). For example, NO_2^- in water of hypersaline ponds and soil of McMurdo Dry Valleys, Antarctica, produced from the NO_3^- photolysis, were characterized by significantly negative $\delta^{15}N$ values (< -80‰) (Peters et al., 2014). However, $\delta^{15}N(NO_2^-)$ in this study was only ~2‰ lower than the $\delta^{15}N(NO_3^-)$ in TSP samples collected during this campaign (on average (-5.3 ± 3.3)‰, Text S1) and that at the QOMS stations (annual average of (-5.1 ± 2.3) ‰) (Wang et al., 2020). The similarity in $\delta^{15}N$ isotopes between NO_2^- and NO_3^- suggests particulate nitrate photolysis is unlikely to be the primary source of the TSP NO_2^-.

In addition to nitrate photolysis, the absorption of HONO on alkaline aerosols (i.e., lofted dust and road salt particles) can also result in accumulation of NO_2^- into the particle phase (Vandenboer et al., 2014a; Chen et al., 2019). For example, *VandenBoer et al.* observed a synchronous enhancement of fine particle NO_2^- (as high as 730 ng m^{-3}) alongside the buildup of HONO (up to 1.37 ppbv) after sunset in an agricultural site (Vandenboer et al., 2014a). However, the levels of HONO in terrestrial background environments, typically on the order of dozens of pptv (Ye et al., 2023), are obviously too low to support the observed unexpectedly high levels of particulate NO_2^- (up to 1300 ng m^{-3}). What is more, previous studies indicated the HONO uptake predominately occurs on fine particles (Wang et al., 2015; Chen et al., 2019; Shang et al., 2021), while our observations indicated NO_2^- only exists in coarse particles.

The uptake of NO_2 on mineral dust has also been identified as a significant route for the formation of particulate NO_2^- or gas-phase HONO (Nie et al., 2012; Ndour et al., 2008). For example, *Nie et al.* found a significantly enhanced NO_2^- in coarse particle during daytime in a dust storm event in Mt. Heng (up to 4.5 μg m^{-3}) (Nie et al., 2012). The proposed mechanism is initiated by photo-enhanced conversion of NO_2 to NO_2^- via photo-produced electrons on surface of dust. Nevertheless, given the relatively small NO_2 uptake coefficients on mineral dust or salt surface (generally lower than 1×10^{-6}) (Yu et al., 2021; Bao et al., 2022; Xuan et al., 2025) and the low concentration of NO_2 in pristine environment of TP (e.g., ~ 140 pptv at Namco (Wang et al., 2023), and would be even lower at Mt. Qomolangma), such high levels of particulate NO_2^- are beyond the capacity of NO_2 heterogeneous reactions.

Other than the above-mentioned rationales, the atmospheric physicochemical processes leading to NO_2^- production would influence both fine and coarse-mode particles, and some of the processes

428 (e.g., HONO uptake) preferentially interact with fine-mode particles. However, the observation

429 indicated NO_2^- only exists in TSP but not $PM_{2.5}$, suggesting atmospheric physicochemical processes

430 are unlikely to account for the elevated levels of NO_2^- in TSP.

4.2 Potential effect of atmospheric pollutants in South Asia via long-range transport

432 There is a growing body of compelling evidence indicating that the elevated aerosol loadings

433 and chemical species in TP during spring, i.e., black carbon (Cong et al., 2015; Kang et al., 2019)

434 and soluble components (Dasari et al., 2023; Bhattarai et al., 2023; Lin et al., 2021; Wang et al.,

435 2020; Zhao et al., 2020) are significantly linked to biomass burning emissions from South Asia,

436 which can penetrate into TP via long range transport. Recently, *Bhattarai et al.* observed

437 synchronously elevated water-soluble nitrogen compounds (i.e., NO_2^-, NH_4^+, NO_3^-), levoglucosan

438 (a molecule marker for biomass burning) and bulk $\delta^{15}N$ signatures in TSP at QOMS station, once

439 upon the arrival of biomass burning plumes from South Asia (Bhattarai et al., 2023). Specially, they

440 found that TSP NO_2^- averaged 60 ng m^{-3} during the spring biomass burning influenced episodes,

441 while NO_2^- was always below the detection limit in other seasons (Bhattarai et al., 2023). This

442 suggests that biomass burning events in South Asia and the subsequent long-range transport could

443 contribute to accumulation of NO_2^- in aerosols in Tibet.

444 In this study, the mass concentrations and compositions of water-soluble ions, including SO_4^{2-},

445 NO_3^-, NH_4^+ and TSP NO_2^-, also varied substantially throughout the springtime campaign (Figure 1).

446 The potential effect of South Asian pollutants on our observations was explored by analyzing the

447 air masses origins during the sampling period. As shown in Figure 5, during the first-half of the

448 campaign (i.e., before April 30th), air masses predominately originated from or passed through

449 northern India and Nepal with intensive human activities and numerous fire hotspots (represented

450 by the dense red dots in Figure 5), indicating the potential impact of South Asia pollutants on aerosol

451 loadings of TP. Correspondingly, elevated concentrations of secondary inorganic ions (i.e., NH_4^+,

452 NO_3^- and SO_4^{2-}) in TSP and $PM_{2.5}$ were observed before April 30th, which are comparable to the

453 values of previous reports in QOMS station when arrived air masses experiencing severe biomass

454 burning emissions (Bhattarai et al., 2023; Lin et al., 2021). Meanwhile, elevated levels of TSP NO_2^-

455 (625 ± 457 ng m^{-3}) was observed during this biomass burning-impacted period, and $\delta^{15}N(NO_2^-)$

456 values exhibited substantial variability. TSP samples collected during daytime of April 27th and night

of April 28th were associated with high NO_2^- concentrations and $\delta^{15}N(NO_2^-)$ values. In comparison, TSP NO_2^- in other samples were significantly ^{15}N-depleted. Assuming that biomass burning emission accounted for the two high $\delta^{15}N(NO_2^-)$ samples (Bhattarai et al., 2023), the observed relatively low $\delta^{15}N(NO_2^-)$ in other samples before April 30th likely indicated the potential contribution from additional emission sources.

From May 1st to May 6th, air masses originated primarily from the inside of the TP or surroundings and none of the fire hotspot was detected at the whole TP and along the air mass trajectories (Figure 5), potentially excluding the influence of biomass burning and anthropogenic emissions during this period. Accompanied by this significant shift in air mass origins, the concentrations of NH_4^+, NO_3^- and SO_4^{2-} in both PM$_{2.5}$ and TSP, as well as the TSP NO_2^- apparently decreased. In particular, NH_4^+ in most PM$_{2.5}$ and TSP samples were below the detection limit during this period. Furthermore, K^+ in PM$_{2.5}$, a common tracer for biomass burning, declined from 269 ± 432 ng m^{-3} before April 30th to 22 ± 12 ng m^{-3} after April 30th, with the difference being statistically significant ($p < 0.05$). Meanwhile, the average TSP NO_2^- also declined significantly from 625 ± 457 ng m^{-3} before April 30th to 147 ± 145 ng m^{-3} after April 30th. Note substantially high levels of TSP NO_2^- were also observed on several days after April 30th, i.e., during daytime of May 3rd (~ 400 ng m^{-3}). Although the TSP NO_2^- concentrations varied in wide range after April 30th, the $\delta^{15}N(NO_2^-)$ was relatively stable and comparable to that determined before April 30th (except for the two high $\delta^{15}N(NO_2^-)$ samples).

In short summary, these results likely suggest the significant impact of South Asia pollutants (i.e., biomass burning emissions) through long-range transport on the TSP NO_2^-, especially for samples collected before April 30th. However, it is difficult for the long-range transport to explain why NO_2^- is predominately present in coarse particles, as fine mode particle is typically easier to be transported in principle. While further studies need to be conducted to find out the exact reasons, one possibility is that the size partition of fine particle NO_2^- toward the coarse mode range during transport. Similar size shifts of NO_3^- have been observed and used to explain the enrichment of NO_3^- in coarse-mode aerosols in marine environment (Matsumoto et al., 2009). In addition, the coarse mode particles in this study contain more alkaline species (Figure 2), which makes nitrite more stable in TSP during the transport or more stably exist in TSP after being uptake when the polluted

air masses reaching TP. For the period after April 30th, since air masses originated from clean regions

with little to no biomass burning sources, other sources of nitrite might be required.
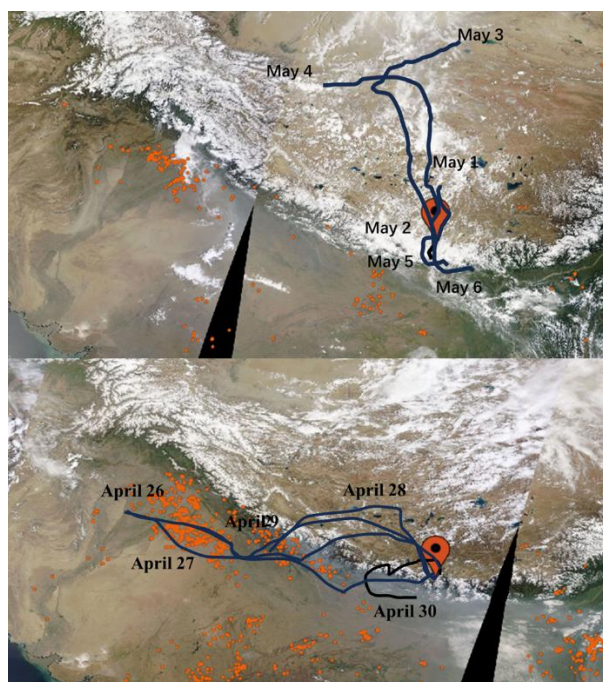
Figure 5. The modelled air-mass back trajectories during "Earth Summit Mission" scientific

expedition in spring 2022 (a: from May 1st to May 6th; b: April 26th to April 30th). The active fire

spots captured by MODIS (https://worldview.earthdata.nasa.gov, the red dots in the figure) are also

presented.

4.3 The potential effects of lofted dust

Previous reports have confirmed that wind-blown mineral dust contributed significantly to

coarse mode aerosols in TP (Kang et al., 2016; Zhang et al., 2021a). Notably, surface soil collected

from the Rongbuk valley is characterized with elevated NO$_2^-$ concentration (up to 180 ng g^{-1}, Table

1). The surface soil NO$_2^-$ is expected to mainly reside in the coarse mode after suspended in the

atmosphere (Drakaki et al., 2022), consistent with our observations that particle NO$_2^-$ was

predominately confined into coarse particle. The unique environment of Rongbuk valley,

characterized by exposed surface soil and strong wind (reaching as high as 9 m/s during this

campaign) could facilitate the resuspension of soil components into the atmosphere. Furthermore,

small localized tornadoes were frequently observed before April 30th, while the snow events

occurred in April 30th would reduce the soil-derived dust emission by increasing the snow coverage

and enriching the soil moisture. In fact, concentrations of Ca^{2+} in TSP, which predominately originate from dust emission, also declined to some extent after April 30th.

In addition, the ~~similarity in~~comparable $\delta^{15}N$ values of NO_2^- between TSP collected after May 1st (-8.0 ± 0.7‰)~~(-7.3 ± 3.1‰)~~ and the surface soil (-10.3 ± 3.0‰) also ~~likely~~ supports that locally ~~emitted~~ resuspended surface soil ~~may~~ is an important ~~contribute~~ contributor to the observed high levels of TSP NO_2^-. But one should note that the oxygen isotopes ($\delta^{18}O$ and $\Delta^{17}O$) of TSP NO_2^- were significantly lower compared to that in soil NO_2^-, indicating that the original soil NO_2^- oxygen isotope may have been modified after resuspension. This discrepancy could be explained by the potential oxygen isotope exchanges between TSP NO_2^- and aerosol liquid water (fractionation effect of $^{18}\varepsilon_{eq} \approx 16‰$ at local temperature, T = 270K, $^{18}\varepsilon_{eq} = -0.12\ T + 48.79$ (Buchwald and Casciotti, 2013)), which tend to deplete both the initial $\delta^{18}O(NO_2^-)$ and $\Delta^{17}O(NO_2^-)$.

We noted the oxygen isotope exchange process between NO_2^- and H_2O also occurs in surface soil. Previous study indicated that in high-altitude arid regions of TP (i.e., >5000m), denitrification process dominated the surface soil NO_2^- production, accounting for ~75% (Wang et al., 2019). Soil NO_2^- generated from denitrification process is expect to inherit the $\Delta^{17}O$ signatures of substrate NO_3^-. In this study, the surface soil $\Delta^{17}O(NO_3^-)$ were positive with average values of 9.6‰ (Table 1). The positive soil $\Delta^{17}O(NO_3^-)$ have been observed on arid environments (Wang et al., 2016), such as desert soil, where the low water moisture favors the preservation of atmospherically derived NO_3^-. One could estimate that soil $\Delta^{17}O(NO_2^-)$ derived from the denitrification would be 9.6‰, nitrite from other sources (e.g., nitrification) should possess zero $\Delta^{17}O$, thus in total nitrite in soil should possess $\Delta^{17}O$ of ~7.2‰ (estimated as $0.75 \times \Delta^{17}O(NO_3^-)$). However, the determined soil $\Delta^{17}O(NO_2^-)$ (3.8‰) is significantly lower compared to the estimated soil $\Delta^{17}O(NO_2^-)$, indicating the occurrence of exchange process between soil water and NO_2^-, which would reduce the soil $\Delta^{17}O(NO_2^-)$ to some extent. The exchange process between soil water and NO_2^- is particularly evident in west slope of Rongbuk Valley, where soil $\Delta^{17}O(NO_2^-)$ is as low as 1.5‰ while soil $\Delta^{17}O(NO_3^-)$ is on average 10.3‰. Soil $\Delta^{17}O(NO_2^-)$ should be erased to near-zero if exchange process between soil water and NO_2^- was efficient. Therefore, the fact that the observed soil $\Delta^{17}O(NO_2^-)$ remain above 0‰ indicates unfavorable conditions for the oxygen isotope exchange process, likely due to the extremely low soil moisture content (~1%) in surface soil (Ma et al., 2023).

533   Upon resuspension into atmosphere, the soil-derived dust aerosols usually exhibited a certain

534   degree of hygroscopicity (Tang et al., 2016; Chen et al., 2020), allowing the absorption of water

535   molecule on dust aerosol. For example, the aerosol water was determined to account for ~20% of

536   the total PM_{10} mass during Saharan dust plumes (Cardoso et al., 2018). Based on laboratory

537   experiment, Tang et al., 2019 reported that Asian dust also exhibited substantial hygroscopic

538   property and revealed that the water-soluble inorganic ions, such as Cl^-, SO_4^{2-} and NO_3^- played a

539   critical role in the absorption of water molecules on dust aerosol (Tang et al., 2019). In the present

540   study, the SO_4^{2-} and NO_3^- account for ~30% of the total mass of water-soluble ions in TSP, implying

541   the potential uptake of water vapor on aerosol surface. In addition to water-soluble ions, the

542   hygroscopicity of mineral dust also depends on the surface areas, and wind-blown dust experiences

543   a substantial increase in surface area after being lifted into the atmosphere, enhancing its capacity

544   for water uptake (Chen et al., 2020; Seisel et al., 2004). The hygroscopicity of dust aerosol is

545   expected to accelerate the oxygen isotope exchanges between NO_2^- and aerosol liquid water. The

546   atmospheric water vapor $\delta^{18}O$ isotope in TP is determined to be significantly negative

547   (approximately -35‰ to -15‰ at a remote site in TP with altitude of ~ 4200m) (Yu et al., 2015).

548   Similarly, the oxygen isotope exchange between NO_2^- and H_2O would also homogenize and erase

549   original soil $\Delta^{17}O(NO_2^-)$ signals, because aerosol liquid water is characterized by negligible $\Delta^{17}O$

550   values (Luz and Barkan, 2005). Consequently, isotope exchange with aerosol water would further

551   reduce both $\delta^{18}O$ and $\Delta^{17}O$ of TSP NO_2^-, effectively masking the original isotopic signature inherited

552   from surface soil.

553   We also noted that NO_2^- in surface soil is significantly lower than NO_3^-, by on average 35 times

554   (Table 1), contrasting with the chemical compositions in TSP. It is important to note that during the

555   complex dust generation and aerosolization processes, water-soluble ions exhibit significant

556   chemical enrichment relative to that in parent soil (Wu et al., 2022; Gao et al., 2023). For example,

557   Wu et al., 2022 reported that contents of nitrate in sand dust-derived PM_{10} is higher than the original

558   soil samples by 2~80 times, while sulphate can be up to 500 times higher than the original soil.

559   Although the enrichment of nitrite has not been evaluated to the extent of our knowledge, we

560   propose that the observed discrepancy of nitrate/nitrite ratio between TSP and surface soil can be

561   reconciled if the nitrite is enriched more efficiently than nitrate during dust aerosolization, i.e., by a

factor of 30. To further assess the potential contribution of resuspended soil to elevated nitrite in TSP, we conducted a rough estimation based on laboratory investigations from Wu et al. (2022). First, the springtime TSP concentrations observed in the nearby QOMS station is used (65.1 ± 50.9 $\mu g\ m^{-3}$; (Liu et al., 2017)), as TSP mass concentrations surrounding the Base camp were not available. Second, we assume the nitrite content in soil-derived coarse particles to be similar to that of nitrate (0.2%) in laboratory-generated dust aerosol from natural sandy and gravel soils (Wu et al., 2022), which is comparable to the soil texture of the Rongbuk Valley. This assumption can also explain the comparable amounts of nitrite and nitrate observed in TSP samples in this study. Results shown that the concentrations of nitrite in TSP can be approximately $130 \pm 102\ ng\ m^{-3}$, on the same order with the observed nitrite concentration in TSP after April 30th ($147 \pm 145\ ng\ m^{-3}$) but substantially lower than that before April 30th ($625 \pm 457\ ng\ m^{-3}$). Therefore, we speculate that the resuspension of surface soil may account for the observed TSP nitrite after April 30th, whereas the biomass burning and soil together co-contributed to the high TSP nitrite before April 30th. This is also consistent with the shift of air mass origins, which clearly indicated that airmasses before April 30th is significantly impacted by the biomass burning emissions, and after April 30th airmasses primarily originated from clean regions. While we acknowledge that this simplistic estimation is subject to substantial uncertainty, it provides a first-order assessment supporting the hypothesis that wind-blown soil dust contributes to coarse-mode particulate nitrite. Previously, wind-blown mineral dust has been verified as a potential source for aerosol water-soluble ions (Engelbrecht et al., 2016; Wu et al., 2022; Wu et al., 2012) and dust aerosol is also recognized as one of the important aerosol types over TP (Pokharel et al., 2019).

5   Conclusion and Implications

Unexpectedly high levels of NO_2^- associated with coarse-particle were observed in the pristine environment at Mt. Qomolangma in the spring, 2022. After examining the potential contributions of various NO_2^- sources with assistance from air mass back-trajectory and isotope analyses, we propose that both soil-derived nitrite and long-range transport of pollutants from South Asia may contribute to coarse-particle NO_2^- during spring at Mt. Qomolangma. This is also consistent with previous reports showing that dust and biomass burning emission through long-range transport from South Asia are the predominant contributors to the springtime aerosol loadings over TP (Zhao et al.,

2020; Pokharel et al., 2019). The nitrite concentrations and isotopes further indicated that soil-derived nitrite likely serves as a baseline source of atmospheric NO_2^-, maintaining the background levels of TSP NO_2^- at this pristine site, reflected by the relatively stable isotopes when soil-derived nitrite predominated. In addition, air masses originating from South Asia would result in elevated levels of NO_2^- observed before April 30th by bringing additional biomass burning and anthropogenic pollutants, as evidenced by the more varied isotopes before April 30th compared to after that day when air mass origins shifted from South Asia to central and north Tibet. However, the detailed mechanisms of nitrite enriched on the coarse particle remain unknown and need further explorations.

In the atmosphere, photolysis of particle nitrite can produce OH radical and NO, the latter is essential for the formation of atmospheric oxidants and secondary aerosols. Moreover, the elevated levels of particle NO_2^- may serve as an important HONO source through the gas-to-particle partition process (Vandenboer et al., 2014a), and the thermodynamic equilibrium between particulate nitrite and HONO ([pN(III)]/[HONO] ratio) is primarily governed by the particle acidity and liquid water content (LWC) in theory (Fountoukis and Nenes, 2007; Vandenboer et al., 2014a; Chen et al., 2019). Based on the observed TSP NO_2^- and estimated ratio of [pN(III)]/[HONO] (from 4.8 to 10.6, Text S2), we can estimate the potential level of atmospheric HONO if the partition ever occurs at this site (Vandenboer et al., 2014b), and result indicates HOHO would be at 8 ~ 15 pptv, on the same order with the observations at a central Tibetan site (~ 30 pptv at Namco (Wang et al., 2023)). Given that TSP concentrations usually reach maximum during spring over TP, i.e., 65 ± 51 μg m^{-3} at the nearby QOMS station (Liu et al., 2017), our findings suggest that the coarse-particle may serve as a potential source of atmospheric HONO and NO_x assuming the TSP are associated with nitrite. Although the coarse-particle tend to deposit rapidly within hours, their potential to influence local atmospheric chemistry remains important to some extent, particularly considering the frequent dust events in TP (loose arid/semiarid surface, sparse vegetation, and strong winds.(Long et al., 2025)) and the ubiquity of long-range transport of biomass burning emissions from South Asia during this season. The impact of the TSP nitrite on the budget of NOx, HONO and OH radicals especially in the background atmosphere could be investigated using regional or global atmospheric transport model, once the detailed mechanism regarding the sources and chemistry of TSP nitrite been elucidated. In summary, our results highlight the need for further investigation into the sources,

620 partitioning, and chemical reactivity of aerosol-phase nitrite, particularly in the pristine Tibetan

621 Plateau, where even small inputs of NO_x or HONO can disproportionately affect oxidant budgets

622 and reactive nitrogen cycling

623

624 **Acknowledgments** We thank Dr. Yunhong Zhou for the help in air mass back trajectory analysis.

625 The authors thank all researchers involved in the "Earth Summit Mission-2022" scientific

626 expedition from Peking University, Hefei Institutes of Physical Science Anhui Institute of Optics

627 and Fine Mechanics of Chinese Academy of Sciences, Minzu University of China.

628 **Financial support** L.G. acknowledges financial support from the National Natural Science

629 Foundation of China (Awards: 41822605 and 41871051), and the National Key R&D Program of

630 China (2022YFC3700701), the Innovation Program for Quantum Science and Technology

631 (2021ZD0303101). Z. Z acknowledges financial support from the National Natural Science

632 Foundation of China (Awards: 42273001), Key Research and Development Plan Project of Anhui

633 Province (2022l07020032). P. C acknowledges financial support from the National Natural Science

634 Foundation of China (Awards: 42371151).

635 **Conflicts of interest**

636 The authors declare that they have no conflicts of interest.

637 **Autor contribution:**

638 L.G designed the research, interpreted the data; L.G and Z.Z prepared the manuscript with

639 contributions from all co-authors; Z.Z., Y.W., C.Y., T.Z., C.Z., Z.J., and P.C., conducted the field

640 sampling and laboratory measurements; L.G, Z.Z., and P.C., acquired funding; L.G., S.K., and C.Y.

641 reviewed and edited the manuscript. All authors have given approval to the final version of the

642 manuscript.

643 **Data availability**

644 The data supporting the findings of this study are available in the archival repository at:
645 https://doi.org/10.6084/m9.figshare.28188320.v1

646 **References**

647 Albertin, S., Savarino, J., Bekki, S., Barbero, A., and Caillon, N.: Measurement report: Nitrogen isotopes

648   ($\delta^{15}N$) and first quantification of oxygen isotope anomalies ($\Delta^{17}O$, $\delta^{18}O$) in atmospheric nitrogen dioxide,

649   Atmos. Chem. Phys., 21, 10477-10497, 10.5194/acp-21-10477-2021, 2021.

650   Andersen, S. T., Carpenter, L. J., Reed, C., Lee, J. D., Chance, R., Sherwen, T., Vaughan, A. R., Stewart,

651   J., Edwards, P. M., and Bloss, W. J. J. S. A.: Extensive field evidence for the release of HONO from the

652   photolysis of nitrate aerosols, Science Advances, 9, eadd6266, 2023.

653   Bao, F., Cheng, Y., Kuhn, U., Li, G., Wang, W., Kratz, A. M., Weber, J., Weber, B., Pöschl, U., and Su,

654   H.: Key Role of Equilibrium HONO Concentration over Soil in Quantifying Soil–Atmosphere HONO

655   Fluxes, Environmental Science & Technology, 56, 2204-2212, 10.1021/acs.est.1c06716, 2022.

656   Bhattarai, H., Wu, G., Zheng, X., Zhu, H., Gao, S., Zhang, Y.-L., Widory, D., Ram, K., Chen, X., and

657   Wan, X.: Wildfire-Derived Nitrogen Aerosols Threaten the Fragile Ecosystem in Himalayas and Tibetan

658   Plateau, Environmental Science Technology, 2023.

659   Bhattarai, H., Zhang, Y.-L., Pavuluri, C. M., Wan, X., Wu, G., Li, P., Cao, F., Zhang, W., Wang, Y., and

660   Kang, S.: Nitrogen speciation and isotopic composition of aerosols collected at Himalayan forest (3326

661   m asl): seasonality, sources, and implications, Environmental Science Technology, 53, 12247-12256,

662   2019.

663   Buchwald, C. and Casciotti, K. L.: Isotopic ratios of nitrite as tracers of the sources and age of oceanic

664   nitrite, Nature Geoscience, 6, 308-313, 10.1038/ngeo1745, 2013.

665   Casciotti, K. L., Böhlke, J. K., McIlvin, M. R., Mroczkowski, S. J., and Hannon, J. E.: Oxygen isotopes

666   in nitrite: Analysis, calibration, and equilibration, Analytical Chemistry, 79, 2427-2436, 2007.

667   Chen, Q., Edebeli, J., McNamara, S. M., Kulju, K. D., May, N. W., Bertman, S. B., Thanekar, S., Fuentes,

668   J. D., and Pratt, K. A.: HONO, Particulate Nitrite, and Snow Nitrite at a Midlatitude Urban Site during

669   Wintertime, ACS Earth and Space Chemistry, 3, 811-822, 10.1021/acsearthspacechem.9b00023, 2019.

670   Cong, Z., Kang, S., Kawamura, K., Liu, B., Wan, X., Wang, Z., Gao, S., and Fu, P.: Carbonaceous

671   aerosols on the south edge of the Tibetan Plateau: concentrations, seasonality and sources, Atmos. Chem.

672   Phys., 15, 1573-1584, 10.5194/acp-15-1573-2015, 2015.

673   Dasari, S., Paris, G., Pei, Q., Cong, Z., and Widory, D.: Tracing the origin of elevated springtime

674   atmospheric sulfate on the southern Himalayan-Tibetan plateau, Environmental Science: Advances, 2,

675   1110-1118, 2023.

676   Decesari, S., Facchini, M., Carbone, C., Giulianelli, L., Rinaldi, M., Finessi, E., Fuzzi, S., Marinoni, A.,

677   Cristofanelli, P., and Duchi, R. J. A. C.: Chemical composition of PM10 and PM1 at the high-altitude

678   Himalayan station Nepal Climate Observatory-Pyramid (NCO-P)(5079 m asl), Atmospheric Chemistry

679   Physics, 10, 4583-4596, 2010.

680   Drakaki, E., Amiridis, V., Tsekeri, A., Gkikas, A., Proestakis, E., Mallios, S., Solomos, S., Spyrou, C.,

681   Marinou, E., Ryder, C. L., Bouris, D., and Katsafados, P.: Modeling coarse and giant desert dust particles,

682   Atmos. Chem. Phys., 22, 12727-12748, 10.5194/acp-22-12727-2022, 2022.

683   Erbland, J., Vicars, W. C., Savarino, J., Morin, S., Frey, M. M., Frosini, D., Vince, E., and Martins, J. M.

684   F.: Air–snow transfer of nitrate on the East Antarctic Plateau Part 1: Isotopic evidence for a photolytically

685   driven dynamic equilibrium in summer, Atmospheric Chemistry and Physics, 13, 6403-6419,

686   10.5194/acp-13-6403-2013, 2013.

687   Fang, Y., Koba, K., Wang, X., Wen, D., Li, J., Takebayashi, Y., Liu, X., and Yoh, M.: Anthropogenic

688   imprints on nitrogen and oxygen isotopic composition of precipitation nitrate in a nitrogen-polluted city

689   in southern China, Atmos. Chem. Phys., 11, 1313-1325, 2011.

690   Felix, J. D. and Elliott, E. M.: Isotopic composition of passively collected nitrogen dioxide emissions:

Vehicle, soil and livestock source signatures, Atmospheric Environment, 92, 359-366, 10.1016/j.atmosenv.2014.04.005, 2014.

Fountoukis, C. and Nenes, A.: ISORROPIA II: a computationally efficient thermodynamic equilibrium model for K^+–Ca^{2+}–Mg^{2+}–NH_4^+–Na^+–SO_4^{2-}–NO_3^-–Cl^-–H_2O aerosols, Atmospheric Chemistry and Physics, 7, 4639-4659, 2007.

Geng, L., Alexander, B., Cole-Dai, J., Steig, E. J., Savarino, J., Sofen, E. D., and Schauer, A. J.: Nitrogen isotopes in ice core nitrate linked to anthropogenic atmospheric acidity change, Proceedings of the National Academy of Sciences, 111, 5808-5812, 2014.

Hastings, M. G., Sigman, D. M., and Lipschultz, F.: Isotopic evidence for source changes of nitrate in rain at Bermuda, Journal of Geophysical Research: Atmospheres, 108, 10.1029/2003jd003789, 2003.

Homyak, P. M., Vasquez, K. T., Sickman, J. O., Parker, D. R., and Schimel, J. P.: Improving nitrite analysis in soils: Drawbacks of the conventional 2M KCl extraction, Soil Science Society of America Journal, 79, 1237-1242, 2015.

Hsu, S. C., Liu, S. C., Huang, Y. T., Chou, C. C., Lung, S. C., Liu, T. H., Tu, J. Y., and Tsai, F.: Long-range southeastward transport of Asian biosmoke pollution: Signature detected by aerosol potassium in northern Taiwan, Journal of Geophysical Research: Atmospheres, 114, 2009.

Immerzeel, W. W., Van Beek, L. P., and Bierkens, M. F.: Climate change will affect the Asian water towers, Science, 328, 1382-1385, 2010.

Jacobi, H.-W., Kleffmann, J. r., Villena, G., Wiesen, P., King, M., France, J., Anastasio, C., and Staebler, R.: Role of nitrite in the photochemical formation of radicals in the snow, Environmental science technology, 48, 165-172, 2014.

Kang, S., Chen, P., Li, C., Liu, B., and Cong, Z.: Atmospheric aerosol elements over the inland Tibetan Plateau: Concentration, seasonality, and transport, Aerosol Air Quality Research, 16, 789-800, 2016.

Kang, S., Zhang, Q., Qian, Y., Ji, Z., Li, C., Cong, Z., Zhang, Y., Guo, J., Du, W., Huang, J., You, Q., Panday, A. K., Rupakheti, M., Chen, D., Gustafsson, Ö., Thiemens, M. H., and Qin, D.: Linking atmospheric pollution to cryospheric change in the Third Pole region: current progress and future prospects, National Science Review, 6, 796-809, 10.1093/nsr/nwz031, 2019.

Keck, L. and Wittmaack, K. J. A. E.: Effect of filter type and temperature on volatilisation losses from ammonium salts in aerosol matter, Atmospheric Environment, 39, 4093-4100, 2005.

Kehrwald, N. M., Thompson, L. G., Tandong, Y., Mosley-Thompson, E., Schotterer, U., Alfimov, V., Beer, J., Eikenberg, J., and Davis, M. E.: Mass loss on Himalayan glacier endangers water resources, Geophysical Research Letters, 35, 2008.

Lau, W. K., Kim, M.-K., Kim, K.-M., and Lee, W.-S.: Enhanced surface warming and accelerated snow melt in the Himalayas and Tibetan Plateau induced by absorbing aerosols, Environmental Research Letters, 5, 025204, 2010.

Lewicka-Szczebak, D., Jansen-Willems, A., Müller, C., Dyckmans, J., and Well, R.: Nitrite isotope characteristics and associated soil N transformations, Sci Rep, 11, 5008, 2021.

Li, S. M.: Equilibrium of particle nitrite with gas phase HONO: Tropospheric measurements in the high Arctic during polar sunrise, Journal of Geophysical Research: Atmospheres, 99, 25469-25478, 1994.

Lin, Zhang, Y.-L., Yu, M., Fan, M.-Y., Xie, F., Zhang, W.-Q., Wu, G., Cong, Z., and Michalski, G.: Formation mechanisms and source apportionments of airborne nitrate aerosols at a Himalayan-Tibetan Plateau site: Insights from nitrogen and oxygen isotopic compositions, Environmental Science Technology, 55, 12261-12271, 2021.

Lin, W., Zhu, T., Song, Y., Zou, H., Tang, M., Tang, X., and Hu, J.: Photolysis of surface O_3 and

production potential of OH radicals in the atmosphere over the Tibetan Plateau, Journal of Geophysical Research, 113, 10.1029/2007jd008831, 2008.

Liu, X.-Y., Koba, K., Koyama, L. A., Hobbie, S. E., Weiss, M. S., Inagaki, Y., Shaver, G. R., Giblin, A. E., Hobara, S., and Nadelhoffer, K.: Nitrate is an important nitrogen source for Arctic tundra plants, Proceedings of the National Academy of Sciences, 115, 3398-3403, 2018.

Lüthi, Z., Škerlak, B., Kim, S.-W., Lauer, A., Mues, A., Rupakheti, M., and Kang, S.: Atmospheric brown clouds reach the Tibetan Plateau by crossing the Himalayas, Atmospheric Chemistry Physics, 15, 6007-6021, 2015.

Luz, B. and Barkan, E.: The isotopic ratios $^{17}O/^{16}O$ and $^{18}O/^{16}O$ in molecular oxygen and their significance in biogeochemistry, Geochimica et Cosmochimica Acta, 69, 1099-1110, 2005.

Ma, Y., Weber, R., Lee, Y. N., Orsini, D., Maxwell-Meier, K., Thornton, D., Bandy, A., Clarke, A., Blake, D., and Sachse, G.: Characteristics and influence of biosmoke on the fine-particle ionic composition measured in Asian outflow during the Transport and Chemical Evolution Over the Pacific (TRACE-P) experiment, Journal of Geophysical Research: Atmospheres, 108, 2003.

Miller, D. J., Chai, J., Guo, F., Dell, C. J., Karsten, H., and Hastings, M. G. J. G. R. L.: Isotopic composition of in situ soil NOx emissions in manure-fertilized cropland, 45, 12,058-012,066, 2018.

Ming, J., Zhang, D., Kang, S., and Tian, W.: Aerosol and fresh snow chemistry in the East Rongbuk Glacier on the northern slope of Mt. Qomolangma (Everest), Journal of Geophysical Research: Atmospheres, 112, 2007.

Morin, S., Savarino, J., Frey, M. M., Yan, N., Bekki, S., Bottenheim, J. W., and Martins, J. M.: Tracing the origin and fate of NOx in the Arctic atmosphere using stable isotopes in nitrate, Science, 322, 730-732, 10.1126/science.1161910, 2008.

Ndour, M., D'Anna, B., George, C., Ka, O., Balkanski, Y., Kleffmann, J., Stemmler, K., and Ammann, M.: Photoenhanced uptake of NO_2 on mineral dust: Laboratory experiments and model simulations, Geophysical Research Letters, 35, 2008.

Nie, W., Wang, T., Xue, L., Ding, A., Wang, X., Gao, X., Xu, Z., Yu, Y., Yuan, C., and Zhou, Z.: Asian dust storm observed at a rural mountain site in southern China: chemical evolution and heterogeneous photochemistry, Atmos. Chem. Phys., 12, 11985-11995, 2012.

Peters, B., Casciotti, K. L., Samarkin, V. A., Madigan, M. T., Schutte, C. A., and Joye, S. B.: Stable isotope analyses of NO_2^-, NO_3^-, and N_2O in the hypersaline ponds and soils of the McMurdo Dry Valleys, Antarctica, Geochimica et Cosmochimica Acta, 135, 87-101, 2014.

Pokharel, M., Guang, J., Liu, B., Kang, S., Ma, Y., Holben, B. N., Xia, X. a., Xin, J., Ram, K., Rupakheti, D., Wan, X., Wu, G., Bhattarai, H., Zhao, C., and Cong, Z.: Aerosol Properties Over Tibetan Plateau From a Decade of AERONET Measurements: Baseline, Types, and Influencing Factors, Journal of Geophysical Research: Atmospheres, 124, 13357-13374, 10.1029/2019jd031293, 2019.

Shang, X., Kang, H., Chen, Y., Abdumutallip, M., Li, L., Li, X., Fu, H., Wang, X., Wang, L., and Wang, X.: $PM_{1.0}$-nitrite heterogeneous formation demonstrated via a modified versatile aerosol concentration enrichment system coupled with ion chromatography, Environmental Science Technology, 55, 9794-9804, 2021.

Tripathee, L., Kang, S., Rupakheti, D., Cong, Z., Zhang, Q., and Huang, J.: Chemical characteristics of soluble aerosols over the central Himalayas: insights into spatiotemporal variations and sources, Environmental Science and Pollution Research, 24, 24454-24472, 2017.

Tripathee, L., Kang, S., Chen, P., Bhattarai, H., Guo, J., Shrestha, K. L., Sharma, C. M., Sharma Ghimire, P., and Huang, J.: Water-soluble organic and inorganic nitrogen in ambient aerosols over the Himalayan

middle hills: Seasonality, sources, and transport pathways, Atmospheric Research, 250, 10.1016/j.atmosres.2020.105376, 2021.

VandenBoer, T., Markovic, M., Sanders, J., Ren, X., Pusede, S., Browne, E., Cohen, R., Zhang, L., Thomas, J., and Brune, W.: Evidence for a nitrous acid (HONO) reservoir at the ground surface in Bakersfield, CA, during CalNex 2010, Journal of Geophysical Research: Atmospheres, 119, 9093-9106, 2014a.

VandenBoer, T. C., Young, C. J., Talukdar, R. K., Markovic, M. Z., Brown, S. S., Roberts, J. M., and Murphy, J. G.: Nocturnal loss and daytime source of nitrous acid through reactive uptake and displacement, Nature Geoscience, 8, 55-60, 10.1038/ngeo2298, 2014b.

Wang, J., Zhang, Y., Zhang, C., Wang, Y., Zhou, J., Whalley, L. K., Slater, E. J., Dyson, J. E., Xu, W., Cheng, P., Han, B., Wang, L., Yu, X., Wang, Y., Woodward-Massey, R., Lin, W., Zhao, W., Zeng, L., Ma, Z., Heard, D. E., and Ye, C.: Validating HONO as an Intermediate Tracer of the External Cycling of Reactive Nitrogen in the Background Atmosphere, Environ Sci Technol, 57, 5474-5484, 10.1021/acs.est.2c06731, 2023.

Wang, K., Hattori, S., Kang, S., Lin, M., and Yoshida, N.: Isotopic constraints on the formation pathways and sources of atmospheric nitrate in the Mt. Everest region, Environmental Pollution, 267, 115274, 2020.

Wang, L., Wen, L., Xu, C., Chen, J., Wang, X., Yang, L., Wang, W., Yang, X., Sui, X., and Yao, L.: HONO and its potential source particulate nitrite at an urban site in North China during the cold season, Science of the Total Environment, 538, 93-101, 2015.

Wang, S., Liu, W., Zhao, S., Wang, C., Zhuang, L., Liu, L., Wang, W., Lu, Y., Li, F., and Zhu, G.: Denitrification is the main microbial N loss pathway on the Qinghai-Tibet Plateau above an elevation of 5000 m, Science of the total environment, 696, 133852, 2019.

Wang, Y. Q. J. M. A.: MeteoInfo: GIS software for meteorological data visualization and analysis, Meteorological Applications, 21, 360-368, 2014.

Wang, Z., Akimoto, H., and Uno, I.: Neutralization of soil aerosol and its impact on the distribution of acid rain over east Asia: Observations and model results, Journal of Geophysical Research: Atmospheres, 107, ACH 6-1-ACH 6-12, 2002.

Xu, B., Cao, J., Hansen, J., Yao, T., Joswia, D. R., Wang, N., Wu, G., Wang, M., Zhao, H., and Yang, W.: Black soot and the survival of Tibetan glaciers, Proceedings of the National Academy of Sciences, 106, 22114-22118, 2009.

Xu, J., Hettiyadura, A. P. S., Liu, Y., Zhang, X., Kang, S., and Laskin, A.: Regional differences of chemical composition and optical properties of aerosols in the Tibetan Plateau, Journal of Geophysical Research: Atmospheres, 125, e2019JD031226, 2020.

Xu, J., Zhang, X., Zhao, W., Zhai, L., Zhao, M., Shi, J., Sun, J., Liu, Y., Xie, C., Tan, Y., Li, K., Ge, X., Zhang, Q., and Kang, S.: High-resolution physicochemical dataset of atmospheric aerosols over the Tibetan Plateau and its surroundings, Earth Syst. Sci. Data Discuss., 2023, 1-45, 10.5194/essd-2023-506, 2023.

Yao, T., Thompson, L. G., Mosbrugger, V., Zhang, F., Ma, Y., Luo, T., Xu, B., Yang, X., Joswiak, D. R., and Wang, W.: Third pole environment (TPE), Environmental Development, 3, 52-64, 2012.

Ye, C., Zhou, X., Zhang, Y., Wang, Y., Wang, J., Zhang, C., Woodward-Massey, R., Cantrell, C., Mauldin, R. L., Campos, T., Hornbrook, R. S., Ortega, J., Apel, E. C., Haggerty, J., Hall, S., Ullmann, K., Weinheimer, A., Stutz, J., Karl, T., Smith, J. N., Guenther, A., and Song, S.: Synthesizing evidence for the external cycling of NOx in high- to low-NOx atmospheres, Nature Communications, 14, 10.1038/s41467-023-43866-z, 2023.

Ye, C., Zhou, X., Pu, D., Stutz, J., Festa, J., Spolaor, M., Tsai, C., Cantrell, C., Mauldin, R. L., 3rd, Campos, T., Weinheimer, A., Hornbrook, R. S., Apel, E. C., Guenther, A., Kaser, L., Yuan, B., Karl, T., Haggerty, J., Hall, S., Ullmann, K., Smith, J. N., Ortega, J., and Knote, C.: Rapid cycling of reactive nitrogen in the marine boundary layer, Nature, 532, 489-491, 10.1038/nature17195, 2016.

Yu, C., Wang, Z., Ma, Q., Xue, L., George, C., and Wang, T.: Measurement of heterogeneous uptake of NO_2 on inorganic particles, sea water and urban grime, Journal of Environmental Sciences, 106, 124-135, 2021.

Yu, W., Tian, L., Ma, Y., Xu, B., and Qu, D.: Simultaneous monitoring of stable oxygen isotope composition in water vapour and precipitation over the central Tibetan Plateau, Atmospheric Chemistry and Physics, 15, 10251-10262, 10.5194/acp-15-10251-2015, 2015.

Zhang, L., Tang, C., Huang, J., Du, T., Guan, X., Tian, P., Shi, J., Cao, X., Huang, Z., and Guo, Q.: Unexpected high absorption of atmospheric aerosols over a western Tibetan Plateau site in summer, Journal of Geophysical Research: Atmospheres, 126, e2020JD033286, 2021a.

Zhang, Y.-L., Zhang, W., Fan, M.-Y., Li, J., Fang, H., Cao, F., Lin, Y.-C., Wilkins, B. P., Liu, X., Bao, M., Hong, Y., and Michalski, G.: A diurnal story of $\Delta^{17}O(NO_3^-)$ in urban Nanjing and its implication for nitrate aerosol formation, npj Climate and Atmospheric Science, 5, 50, 10.1038/s41612-022-00273-3, 2022.

Zhang, Z., Jiang, Z., Guan, H., Liang, Y., Zheng, N., and Guo, W.: Isotopic evidence for the high contribution of wintertime photochemistry to particulate nitrate formation in Northern China, Journal of Geophysical Research: Atmospheres, 126, e2021JD035324, 2021b.

Zhang, Z., Zeng, Y., Zheng, N., Luo, L., Xiao, H., and Xiao, H.: Fossil fuel-related emissions were the major source of NH_3 pollution in urban cities of northern China in the autumn of 2017, Environmental Pollution, 113428, 2020.

Zhao, C., Yang, Y., Fan, H., Huang, J., Fu, Y., Zhang, X., Kang, S., Cong, Z., Letu, H., and Menenti, M.: Aerosol characteristics and impacts on weather and climate over the Tibetan Plateau, National Science Review, 7, 492-495, 2020.

Zhou, L., Zou, H., Ma, S., Li, P., Zhu, J., and Huo, C.: Vertical air mass exchange driven by the local circulation on the northern slope of Mount Everest, Advances in Atmospheric Sciences, 28, 217-222, 2011.

Zhou, T., Jiang, Z., Zhou, J., Zhao, W., Wu, Y., Yu, H., Li, W., Zhang, Z., Su, G., Ma, T., and Geng, L.: Fast and Efficient Atmospheric NO_2 Collection for Isotopic Analysis by a 3D-Printed Denuder System, Anal Chem, 94, 13215-13222, 10.1021/acs.analchem.2c02839, 2022.

Zhu, T., Lin, W., Song, Y., Cai, X., Zou, H., Kang, L., Zhou, L., and Akimoto, H.: Downward transport of ozone-rich air near Mt. Everest, Geophysical Research Letters, 33, 2006.

Zong, Z., Sun, Z., Xiao, L., Tian, C., Liu, J., Sha, Q., Li, J., Fang, Y., Zheng, J., and Zhang, G.: Insight into the Variability of the Nitrogen Isotope Composition of Vehicular NOx in China, Environ. Sci. Tech., 54, 14246-14253, 10.1021/acs.est.0c04749, 2020.

Zou, H., Zhou, L., Ma, S., Li, P., Wang, W., Li, A., Jia, J., and Gao, D.: Local wind system in the Rongbuk Valley on the northern slope of Mt. Everest, Geophysical Research Letters, 35, https://doi.org/10.1029/2008GL033466, 2008.

Uncategorized References

Cardoso, J., Almeida, S. M., Nunes, T., Almeida-Silva, M., Cerqueira, M., Alves, C., Rocha, F., Chaves, P., Reis, M., and Salvador, P.: Source apportionment of atmospheric aerosol in a marine dusty environment by ionic/composition mass balance (IMB), Atmospheric Chemistry and Physics, 18, 13215-

13230, 2018.

Chai, J., Dibb, J. E., Anderson, B. E., Bekker, C., Blum, D. E., Heim, E., Jordan, C. E., Joyce, E. E., Kaspari, J. H., and Munro, H.: Isotopic evidence for dominant secondary production of HONO in near-ground wildfire plumes, Atmospheric Chemistry and Physics, 21, 13077-13098, 2021.

Chai, J., Miller, D. J., Scheuer, E., Dibb, J., Selimovic, V., Yokelson, R., Zarzana, K. J., Brown, S. S., Koss, A. R., and Warneke, C.: Isotopic characterization of nitrogen oxides (NO x), nitrous acid (HONO), and nitrate (pNO 3−) from laboratory biomass burning during FIREX, Atmospheric Measurement Techniques, 12, 6303-6317, 2019.

Chen, L., Peng, C., Gu, W., Fu, H., Jian, X., Zhang, H., Zhang, G., Zhu, J., Wang, X., and Tang, M.: On mineral dust aerosol hygroscopicity, Atmospheric Chemistry and Physics, 20, 13611-13626, 2020.

Engelbrecht, J. P., Moosmüller, H., Pincock, S., Jayanty, R., Lersch, T., and Casuccio, G.: Mineralogical, chemical, morphological, and optical interrelationships of mineral dust re-suspensions, Atmospheric Chemistry and Physics, 16, 10809-10830, 2016.

Fang, T., Guo, H., Verma, V., Peltier, R., and Weber, R.: PM 2.5 water-soluble elements in the southeastern United States: automated analytical method development, spatiotemporal distributions, source apportionment, and implications for heath studies, Atmospheric Chemistry and Physics, 15, 11667-11682, 2015a.

Fang, Y., Koba, K., Makabe, A., Takahashi, C., Zhu, W., Hayashi, T., Hokari, A. A., Urakawa, R., Bai, E., and Houlton, B. Z.: Microbial denitrification dominates nitrate losses from forest ecosystems, Proceedings of the National Academy of Sciences, 112, 1470-1474, 2015b.

Frey, M. M., Savarino, J., Morin, S., Erbland, J., and Martins, J. M. F.: Photolysis imprint in the nitrate stable isotope signal in snow and atmosphere of East Antarctica and implications for reactive nitrogen cycling, Atmos. Chem. Phys., 9, 8681-8696, 10.5194/acp-9-8681-2009, 2009.

Gao, Q., Zhu, S., Zhou, K., Zhai, J., Chen, S., Wang, Q., Wang, S., Han, J., Lu, X., and Chen, H.: High enrichment of heavy metals in fine particulate matter through dust aerosol generation, Atmospheric Chemistry and Physics, 23, 13049-13060, 2023.

Liu, B., Cong, Z., Wang, Y., Xin, J., Wan, X., Pan, Y., Liu, Z., Wang, Y., Zhang, G., Wang, Z., Wang, Y., and Kang, S.: Background aerosol over the Himalayas and Tibetan Plateau: observed characteristics of aerosol mass loading, Atmospheric Chemistry and Physics, 17, 449-463, 10.5194/acp-17-449-2017, 2017.

Long, H., Cheng, L., Yang, F., and Zhang, G.: Temperature regulates dust activities over the Tibetan Plateau, The Innovation, 6, 2025.

Ma, Y., Xie, Z., Ma, W., Han, C., Sun, F., Sun, G., Liu, L., Lai, Y., Wang, B., and Liu, X.: QOMS: a comprehensive observation station for climate change research on the top of Earth, Bulletin of the American Meteorological Society, 104, E563-E584, 2023.

Matsumoto, K., Minami, H., Uyama, Y., and Uematsu, M.: Size partitioning of particulate inorganic nitrogen species between the fine and coarse mode ranges and its implication to their deposition on the surface ocean, Atmospheric Environment, 43, 4259-4265, 2009.

Seisel, S., Lian, Y., Keil, T., Trukhin, M. E., and Zellner, R.: Kinetics of the interaction of water vapour with mineral dust and soot surfaces at T= 298 K, Physical Chemistry Chemical Physics, 6, 1926-1932, 2004.

Tang, M., Cziczo, D. J., and Grassian, V. H.: Interactions of Water with Mineral Dust Aerosol: Water Adsorption, Hygroscopicity, Cloud Condensation, and Ice Nucleation, Chemical Reviews, 116, 4205-4259, 10.1021/acs.chemrev.5b00529, 2016.

Tang, M., Zhang, H., Gu, W., Gao, J., Jian, X., Shi, G., Zhu, B., Xie, L., Guo, L., and Gao, X.: Hygroscopic properties of saline mineral dust from different regions in China: Geographical variations, compositional dependence, and atmospheric implications, Journal of Geophysical Research: Atmospheres, 124, 10844-10857, 2019.

Vicars, W. C. and Savarino, J.: Quantitative constraints on the ^{17}O-excess (Δ^{17}O) signature of surface ozone: Ambient measurements from 50°N to 50°S using the nitrite-coated filter technique, Geochimica et Cosmochimica Acta, 135, 270-287, 10.1016/j.gca.2014.03.023, 2014.

Wang, F., Ge, W., Luo, H., Seo, J.-H., and Michalski, G.: Oxygen-17 anomaly in soil nitrate: A new precipitation proxy for desert landscapes, Earth and Planetary Science Letters, 438, 103-111, 2016.

Wu, F., Zhang, D., Cao, J., Xu, H., and An, Z.: Soil-derived sulfate in atmospheric dust particles at Taklimakan desert, Geophysical research letters, 39, 2012.

Wu, F., Cheng, Y., Hu, T., Song, N., Zhang, F., Shi, Z., Hang Ho, S. S., Cao, J., and Zhang, D.: Saltation–sandblasting processes driving enrichment of water-soluble salts in mineral dust, Environmental Science & Technology Letters, 9, 921-928, 2022.

Xuan, H., Liu, C., Zhang, P., Chu, B., Liang, L., Ma, Q., and He, H.: A Review of Laboratory Studies on the Heterogeneous Chemistry of NO2: Mechanisms and Uptake Kinetics, The Journal of Physical Chemistry A, 2025.

Zhang, Z., Zhou, T., Jiang, Z., Ma, T., Su, G., Ruan, X., Wu, Y., Cao, Y., Wang, X., Liu, Z., Li, W., Zhang, H., Lin, M., Liu, P., and Geng, L.: High-Resolution Measurements of Multi-Isotopic Signatures (δ^{15}N, δ^{18}O, and Δ^{17}O) of Winter NO2 in a Megacity in Central China, Environmental Science & Technology, 59, 3634-3644, 10.1021/acs.est.4c07724, 2025.